MODAL IDENTIFICATION OF A BRIDGE-ABUTMENT SYSTEM USING FORCED VIBRATION TESTING

L.S. Hogan[1], L.M. Wotherspoon[2], S. Beskhyroun[3] and J.M. Ingham[4]

SUMMARY

During the 2010 M_w7.1 Darfield earthquake, the single span Davis Road Bridge located 5 km southeast of Lincoln, New Zealand, sustained significant lateral spreading damage to the western approach. While lateral spreading resulted in up to 450 mm of approach settlement and evidence of damage to the pile foundations, the bridge superstructure sustained no significant damage. Prior to reinstating traffic, the bridge was used for full scale dynamic testing to characterise the influence of different substructure components on the lateral dynamic behaviour of the bridge superstructure.

The bridge was characterised using an eccentric mass shaker and an array of accelerometers to perform lateral forced vibration testing in both the transverse and longitudinal directions. Modal properties were extracted from these tests using multiple system identification algorithms. The experimental testing and system identification methodology are described here. Forced vibration testing was able to detect one mode in each principal direction of the bridge, with the fundamental modes for the transverse and longitudinal direction occurring at a period of 0.118 s and 0.092 s respectively. The torsional response found during the transverse direction shaking was most likely due to the effect of gap opening around the piles on the western abutment, while the longitudinal response was dominated by the approach soil.

INTRODUCTION

Abutments provide large interfaces between a bridge superstructure and the surrounding soil. This interface contributes significantly to the overall stiffness and damping of a bridge system when loaded seismically, especially for short bridges [1-4]. Due to the complicated nature of abutment-embankment interaction, one of the inherent difficulties when modelling this effect is verifying the validity of the model used as different modelling approaches can give wide variations in stiffness distribution, modal properties and damping [5, 6]. While laboratory studies have provided insight as to how well the model describes the physical behaviour [7, 8], ideally testing would be carried out on full scale specimens during in-service conditions. Forced vibration testing of in-situ structures allows for this type of verification. Forced vibration testing has been used to determine dynamic characteristics of bridges for many decades, [9-11] but most studies have investigated vertical excitation of in-situ bridges or lateral excitation of bridge components [12-14]. In-situ lateral forced vibration testing has been performed on a large single span box girder with monolithic abutments and spread footings [15], but there is a paucity of work investigating the response of in-situ bridges with seat type abutments and deep foundations when subjected to lateral forced vibration testing.

Figure 1: ***Overview of Canterbury region with location of the Davis Road Bridge.***

[1] *PhD Candidate, Dept. of Civil & Environmental Engineering, University of Auckland, Auckland, New Zealand*

[2] *EQC Research Fellow, Dept. of Civil & Environmental Engineering, University of Auckland, Auckland, New Zealand*

[3] *EQC Research Fellow, Dept. of Civil & Environmental Engineering, University of Auckland, Auckland, New Zealand*

[4] *Associate Professor, Dept. of Civil & Environmental Engineering, University of Auckland, Auckland, New Zealand*

Figure 2: Site overview of Davis Road Bridge.

The dynamic behaviour of a single span pile supported bridge with seat type abutments was investigated using forced vibration testing on the single span Davis Road Bridge in South Lincoln, Canterbury. The bridge suffered damage to the western approach during the 2010 Darfield earthquake, and upon completion of remediation works, it became available as an in-situ test specimen before traffic was reinstated. Because the bridge was single span, it provided an opportunity to investigate the influence of different substructure components on the dynamic response of the bridge superstructure without the complications of load sharing between piers. The forced vibration testing program and system identification process used to determine the modal properties of this bridge, along with key findings from the testing, are described here.

DAVIS ROAD BRIDGE

The Davis Road Bridge, located approximately 5 km southeast of Lincoln, Canterbury (Figure 1). Constructed in 2005, the bridge services rural traffic crossing the Halswell River between Davis Road and River Road (Figure 2). The single span bridge has overall dimensions of 17.5 m long and 7.0 m wide. The superstructure consists of six 1,144 x 575 mm double hollow core precast concrete units 16.9 metres long. The units are post-tensioned together in the transverse direction at the abutments and at mid-span and support a 75 mm thick asphalt wearing surface. Guardrails are comprised of 100 x 200 mm timber posts 1.0 m high, at 2.0 m centres supporting a 200 x 50 mm barrier rail.

Abutments are of the seat type with backwalls which vary in height from 979-1,182 mm to achieve a 3% cross fall (Figure 4). Backwall widths vary from 150 mm at the superstructure face to 500 mm at the superstructure seat-type support. Precast superstructure units are separated from the backwalls by 20 mm of flexible rubberized sealant. Each abutment is founded on six 275 x 275 x 17,000 mm precast concrete piles spaced at 1,155 mm centres. Abutments also include a 2.0 m long settlement slab under the approach located approximately 1.0 m below the deck surface. The superstructure is supported by 12 mm thick neoprene pads and is connected to each abutment with five 800 mm long anchors located in the grout keys between precast units (Figure 5).

The soil profile at each abutment was characterised with two CPT tests that were performed at each of the bridge approaches [16] (Figure 3). The top 8 m of the soil profile is dominated by sand and silty-sand layers, while between 8 and 13 m, the profile is dominated by silt layers. These layers are underlain by a sandy gravel layer in which the piles are founded. The water table was approximately 3 m below the ground level.

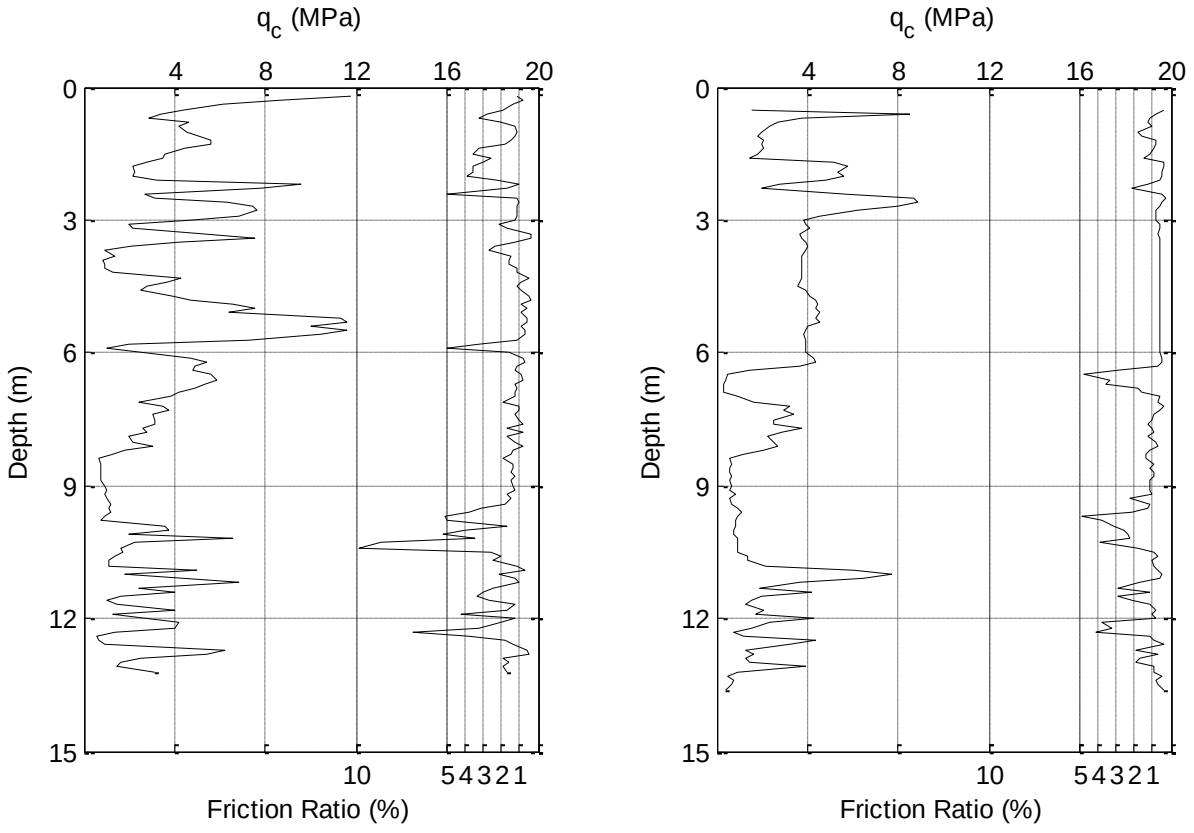

Eastern Approach ***Western Approach***

Figure 3: CPT logs taken at the Davis Road Bridge approaches.

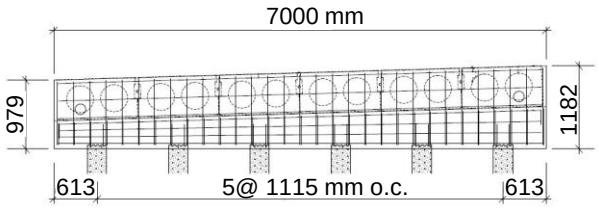

Figure 4: ***Transverse section of Davis Road Bridge showing piles and double hollow core units. All dimensions are in millimetres.***

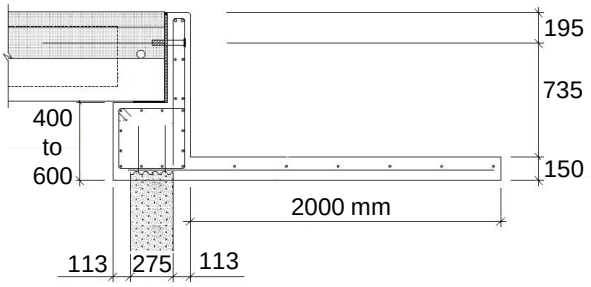

Figure 5: ***Abutment and friction slab section of Davis Road Bridge. All dimensions are in millimetres.***

Earthquake Induced Damage

During the 2010 M_w 7.1 Darfield earthquake, the Davis Road Bridge suffered severe damage to the western approach [17]. Lateral spreading of the river bank resulted in subsidence over a length of several hundred metres around the bridge (Figure 6). A survey of settlement damage taken after the event revealed subsidence at the western approach of up to 455 mm (Figure 7).

Soil on the river side of the piles moved up to 200 mm away from the pile face due to lateral spreading, with the gap between the soil and pile opening up to a depth of 0.7 m (Figure 8). Removal of approach soil revealed that the bank side of the western abutment backwall had cracked across the width of the abutment at approximately 0.5 m below the deck. Additionally, the back wall rotated approximately 4° to close the 20 mm gap between the bottom of the precast deck units and the abutment backwall. Damage sustained at this location was expected as backwalls of seat type abutments are often designed as sacrificial elements [18]. The superstructure, piles and eastern abutment showed no other obvious signs of distress. It is possible that there was damage to the piles at the interface between liquefied and non-liquefied layers, but this assumption was unable to be ascertained without additional subsurface investigations. In the days following the earthquake, the western approach was built up with gravel, and traffic was reinstated.

Liquefaction triggering analysis for the soil profile at each abutment was carried out following the methodology outlined in Youd *et al.* [19]. At the LINC strong motion station, located approximately 5 km nearer the fault rupture of the Darfield earthquake than the Davis Road Bridge, the peak ground acceleration (PGA) was measured to be 0.43g [20].

Using a PGA of 0.3g for the Davis Road site, Figure 9 indicates that liquefied layers were evident at both abutments. Varying the PGA by ± 0.1g resulted in similar liquefied layer thicknesses and depths at both abutments. At the eastern abutment, on the outer river bank, a few thin layers were expected to liquefy, with the largest being a half metre thick

Figure 6: ***Lateral spreading induced settlement of the western approach.***

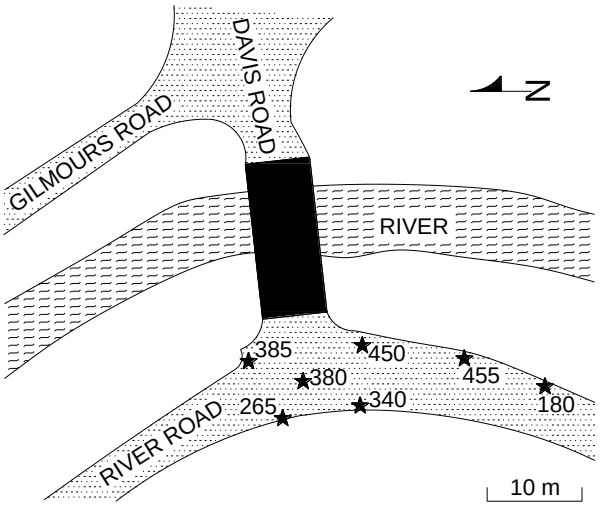

Figure 7: ***Survey of settlements at western approach of the bridge. Stars represent survey points and adjacent values are settlements in millimetres.***

Figure 8: ***Lateral spreading induced gapping at the pile face of western abutment.***

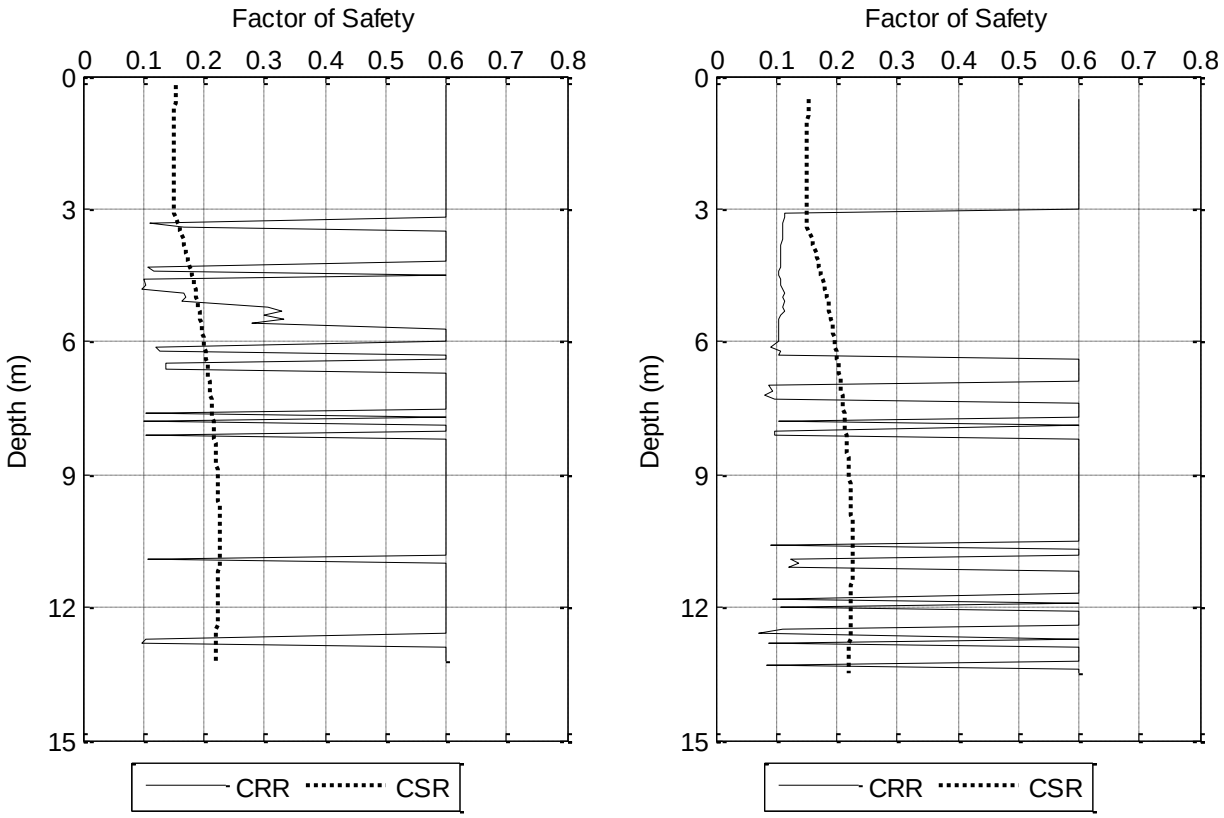

Eastern Approach ***Western Approach***

Figure 9: Liquefaction triggering analysis of Davis Road Bridge approach material by comparison of cyclic stress ratio (CSR) and cyclic resistance ratio (CRR).

layer at approximately 4 m depth. Following the Darfield earthquake, there was no evidence of movement at this riverbank, as the main liquefiable layer was below the base of the free face. At the western abutment, on the inner river bank, there was a 3 m thick layer that was expected to liquefy at a depth of 3 m, which clearly relates to the significant lateral spreading observed at this approach. If the groundwater depth at this location was shallower, the liquefiable layer at the western approach would have further increased in thickness.

The characteristics at the Davis Road Bridge site are similar to those identified at multiple bridge locations in Christchurch, where more damage was also observed on the inner banks of the river due to the lower energy depositional environment than the outer banks [21].

During the M_w 6.2 Christchurch earthquake, the LINC strong motion station, located approximately 5 km further away from the epicentre than the Davis Road site, recorded a PGA of 0.16g [20]. For an earthquake of this magnitude the minimum PGA required for triggering of liquefaction at the western abutment was equal to 0.2g. This analysis is consistent with post-earthquake reconnaissance of the bridge in that evidence of minor liquefaction was observed. Gapping which had formed when material spread away from the pile faces during the Darfield earthquake increased an average of 50 mm away from the pile face and increased in depth by 100 mm. No additional damage to the superstructure was observed. Several months after the Christchurch earthquake, the western approach was remediated, but no improvement was made to the material which had spread away from the piles (Figure 10).

Figure 10: Remediated western approach.

Figure 11: Shaker and accelerometers set up on bridge.

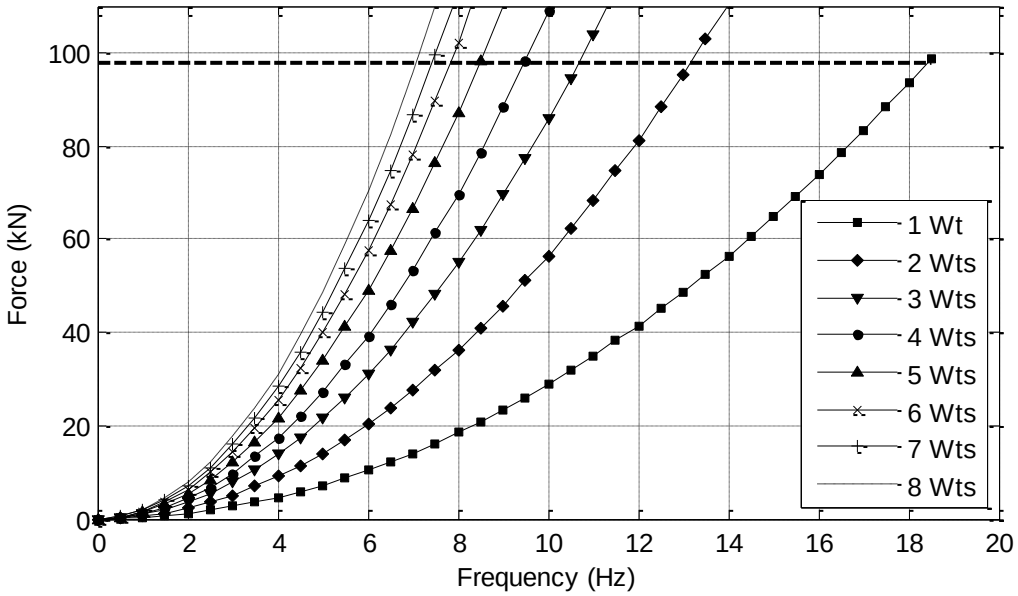

Figure 9: Eccentric mass shaker force output with varying driver frequency.

FORCED VIBRATION TESTING

Experimental Set Up

Forced vibration testing was performed on the bridge using an ANCO Model MK-140-10-50 eccentric mass shaker anchored at mid-span of the bridge (Figure 11). The shaker consisted of a series of 15.5 kg steel weights bolted onto two counter-rotating flywheels controlled by a variable speed three phase induction motor. 440 V power was supplied by a 40 kVA diesel generator located approximately 20 m away from the east abutment. The shaker provided unidirectional frequency dependant loading (P) with time (t) described by the following relationship:

$$P(t) = 2mR\omega^2 \sin(\omega t) \quad (1)$$

where m = total mass being rotated;
R = radius of eccentricity; and
ω = angular frequency of mass given by 2π x driver frequency.

The force output capacity of the shaker was 98 kN.

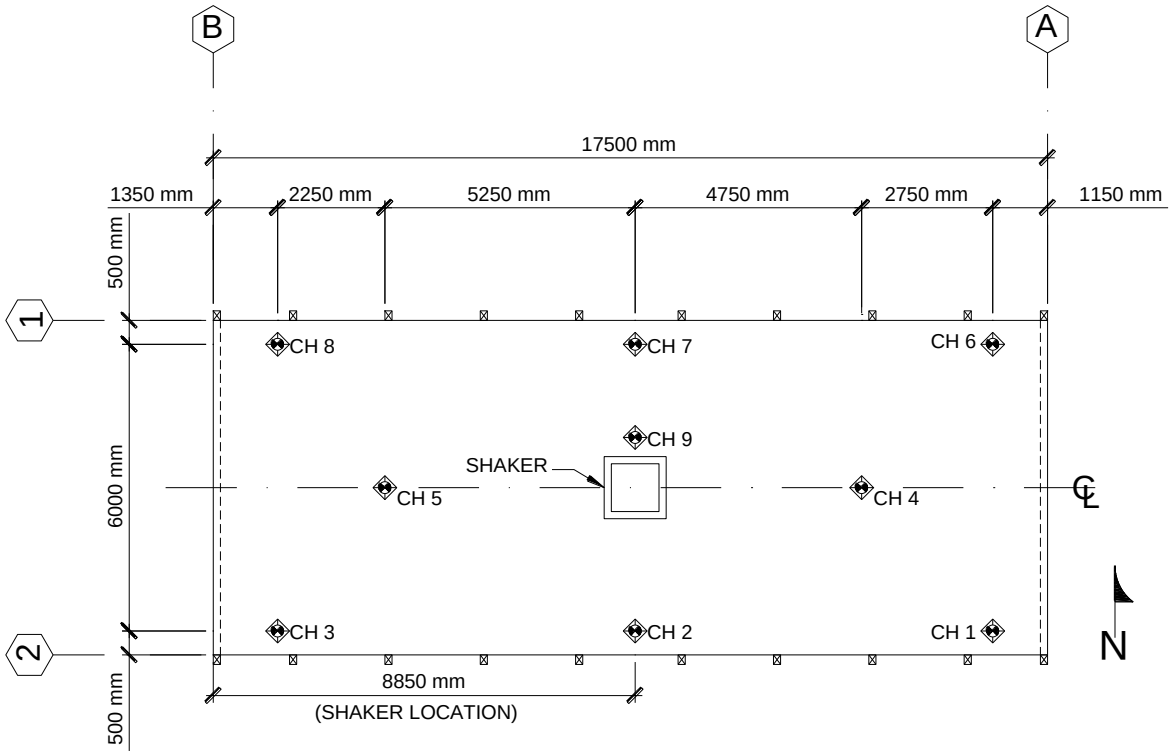

Figure 10: Sensor locations for forced vibration tests.

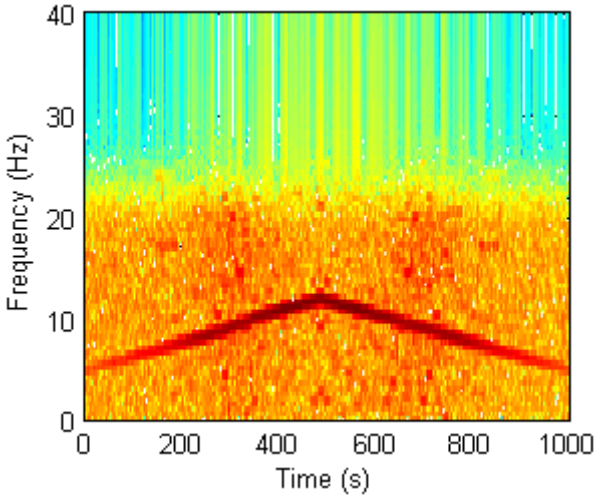

Figure 11: Spectogram of non-normalized forced vibration data.

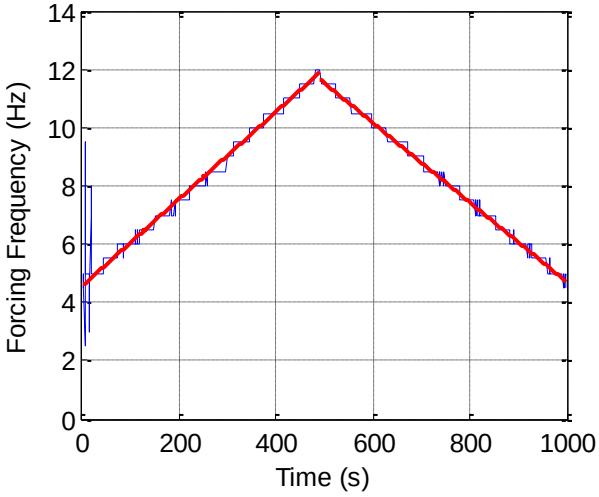

Figure 12: Noisy excitation frequency with respect to time and robust linear regression lines used for smoothing.

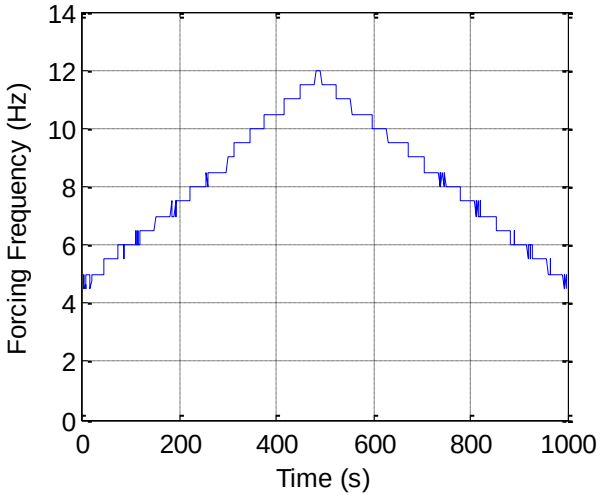

Figure 13: Smoothed excitation frequency.

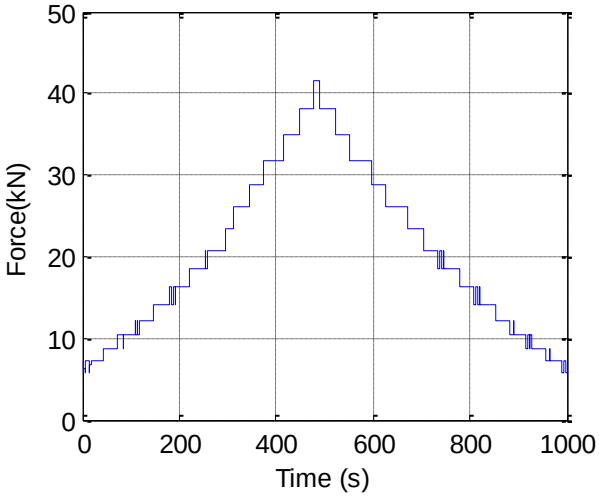

Figure 14: Calculated force input from smoothed excitation frequency.

Figure 12 shows the frequency dependant force output for different sets of weights per flywheel at various diver frequencies.

The bridge response to the shaker excitation was measured using nine uniaxial accelerometers aligned in the direction of shaking (Figure 13) sampling at 256 Hz. Channels 1-8 were used to determine modal properties of the bridge while channel 9 was used as a reference to determine the force input from the shaker.

The bridge was excited in both principal directions by sweeping through a range of frequencies with one 15.5 kg weight attached to each flywheel. Because the bridge was only available to test for six hours, the number of tests that could be performed was limited to eight total and with only one weight configuration. Four frequency sweeps were performed in the transverse direction beginning at 0 Hz, sweeping up to 12 Hz and back down to 0 Hz. Maximum force input was 40 kN. Excitation frequency was increased in 0.2 Hz increments, and each frequency increment was held for ten seconds with a five second ramp up time from the previous excitation frequency. This excitation protocol allowed the bridge to achieve steady state response for each excitation frequency increment while reducing the overall time needed to perform each test. These sweeps were repeated three times in the longitudinal direction with a fourth test sweeping only between 0-16 Hz without a sweep back to zero. The maximum force input for this final test was 55 kN.

Signal Processing

Because shaker excitation force increased exponentially with increasing frequency, the acceleration records needed to be force normalized before performing analysis to avoid spurious modal identifications at high frequencies caused by larger input forces. As shaker force was not measured directly, a method to approximate force input for initial system identification was used.

Due to the proximity of channel 9 to the shaker, the accelerations recorded at this location were used to estimate force input from the shaker. For each test, acceleration records from channel 9 were filtered with a 20 Hz low pass digital filter. A short time Fourier transform was performed on the filtered record and a spectrogram was plotted to determine frequency content at each time step (Figure 14). Time steps were determined by the sampling rate. The dark line that peaks at approximately 500 s in Figure 14 represents the excitation frequency content of the test as it changes with increasing test duration.

The maximum frequency at each time step of the spectrogram was determined and plotted. Figure 15 shows that for higher frequencies, i.e. frequencies with larger force inputs, the shaker excitation followed an approximately step wise linear increase in excitation frequency as was used in the excitation protocol. At the beginning of the acceleration record, where the shaker was exciting the bridge at lower frequencies, there is more scatter in the determined maximum loading frequency. This scatter was typical for all the tests at lower shaker excitation frequencies and arises from electrical noise interfering with the correct identification of excitation frequency from the spectrogram. This noise was smoothed by determining the maximum loading frequency of the test and performing a linear regression from the beginning of the excitation signal to the maximum frequency and from the maximum frequency to the end of the signal (Figure 15). The linear regressions were calculated using a robust least-squares method with bi-square weights to reduce residuals as this method was less sensitive to outliers than the ordinary least squares method. A criterion loop based upon the magnitude of the residuals between the signal and the regression line was used to remove the outliers and smooth the forcing frequency plot (Figure 16). The smoothed forcing frequency plot was used to determine force output at each time step (Figure 17). The acceleration records from channels 1-8 (Figure 15) were divided by the calculated force output and the force-normalized acceleration records used for modal extraction (Figure 16). This process was repeated for each shaker test performed in both directions.

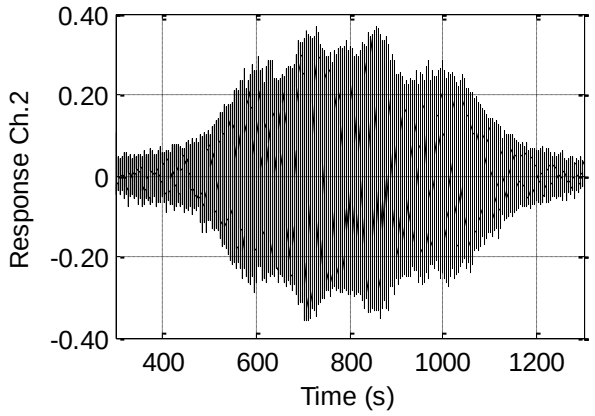

Figure 15: Sample acceleration record prior to force normalization.

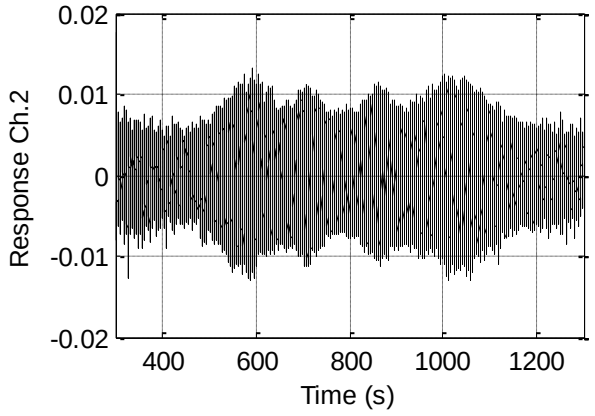

Figure 16: Sample acceleration record after force normalization.

Analysis Methods

The forced vibration data was analysed using a MATLAB based system identification toolbox (SIT) developed at the University of Auckland [22]. SIT was used for both signal processing of the captured acceleration data and for the extraction of mode shapes and natural periods. Analysis of modal properties was performed in two phases. Firstly plausible modes were identified using the entire force-normalized acceleration records from each test. Then the analysis was repeated using the non-force-normalized acceleration data trimmed to only include excitations in a narrow frequency band centred around the mode identified in the previous step. For both phases of modal identification, mode shapes were selected using a rigorous acceptance methodology to avoid biased modal identification.

The data set for each test was then subjected to five different system identification algorithms which were used to find natural frequencies and mode shapes. Three of the five algorithms were frequency domain based and included peak picking (PP), frequency domain decomposition (FDD) [23], and enhanced frequency domain decomposition (EFDD) [24]. A Hamming window size of 4096 was used to calculate singular value decomposition (SVD) for these methods as this window size was found to provide the best resolution, while reducing inaccuracies created by zero padding.

The two time domain based algorithms applied were both variations of the stochastic subspace identification (SSI) method [25]. In both methods the algorithm was run fifty times starting with a Hankel Matrix of size 40 and system order of 100 which reduced by two with each iteration until the final iteration was run with a system order of two. Stable poles identified in each of these iterations were compared by one of two methods. In the first variation of SSI, the stable poles identified around the singular values generated from the SVD were compared. If two consecutive poles within ± 0.25 Hz of the singular value had frequencies within 10% and a modal assurance criteria (MAC) value [26] greater than 0.95 both poles were kept and averaged. If both poles did not meet these criteria then the first pole was discarded and the second pole was compared to the subsequent one. This series of comparisons was continued until all stable poles in the frequency range had been compared and averaged. The resulting mode shape and natural frequency are the combination of several stable poles and therefore provided a robust method of system identification.

While the first method used singular values to identify stable poles, the second variation of SSI breaks up the entire frequency range tested into 0.5 Hz bands. Stable poles are compared within each band and averaged using the same method as the previous SSI variation. Those bands with the most stable poles are considered to contain true modes. The true modes identified from these stable poles are then used to compare to the modal properties found from the other algorithms used in the system identification analysis.

The SIT was used to calculate four modes for each system identification method in order to correctly identify the first translational modes in each direction from the force-normalized acceleration records. Modes were differentiated between true structural response and false noise modes using a two-step process. First power spectral densities (PSD) were calculated for several channels and resonant frequencies were identified. A visual inspection of the generated mode shapes was then performed. If the mode shape did not include impossibilities, such as the rigid deck moving in two different directions simultaneously, and the corresponding eigenfrequencies were close to the resonant frequencies identified in the PSD, then the mode was considered to be a true mode.

Once plausible modes were identified from the preliminary modal extraction, the acceleration records were prepared for a refined extraction of modal properties. Acceleration records from the non-force-normalized data were trimmed to include only accelerations over ±1 Hz of the modal frequency identified in the preliminary analysis, which equated to approximately 200 s for each test. Stable poles identified by SSI were chosen using the same criteria for both series of tests. Consecutive poles were selected within ± 0.05 Hz of the singular value or median frequency band, having frequencies within 1% and a MAC value within 0.09.

Once the true mode was established for a given system identification method, MAC values and differences in identified frequencies were compared between the sweeps of each test to determine repeatability. Modes shapes were accepted if they had a MAC value of 0.95 or higher and the identified eigenfrequencies were within 5%. Using these criteria, 97% of mode shapes generated by the system identification algorithms were accepted. These mode shapes were then averaged and compared to the average mode shapes generated by the other methods. Finally, the compiled mode shapes from each method were averaged together to generate a robustly determined mode shape.

Identified Modes

After the data gathered from the sweeps was analysed and the false modes discarded, modes were identified in each direction for the bridge. This modal data was used to provide an insight into the influence of the different substructure components (approach soil mass, settlement slab, and pile foundations) on the overall bridge response.

In the longitudinal direction the bridge had a natural period of 0.092 s and a mode shape dominated by translational motion (Figure 17). The two channels at mid-span had modal amplitudes which were 40% lower than those located near the abutment. Because only motion in the longitudinal direction was measured, the likely cause of the lower amplitude measured was vertical movement of the deck due to a coupled elastic buckling mode.

This longitudinal mode is approximately symmetrical about the longitudinal axis of the bridge, despite the varying depth of gap opening at the pile faces due to the western abutment damage. The uniformity of motion arises most likely due to the approach soil behind the abutment dominating the response in the longitudinal direction rather than the pile foundation system. This soil mass provides passive resistance along the abutment backwall, while the soil overburden on the settlement slab develops a frictional stiffness component at the interface between the soil and the slab. With the forced vibration loads applied to the bridge deck, much of this load would be transferred into the approach material behind the abutment before being transferred into the pile foundation system underneath. This load transfer mechanism is shown schematically in Figure 18. In this mechanism, the abutment will tend to back rotate during loading and deformations will concentrate at the thin section of the backwall where the bridge deck is anchored, applying pressure to the approach soil. The effect of this applied pressure was identified indirectly during testing, with surface vibrations noticeable several metres away from the abutments.

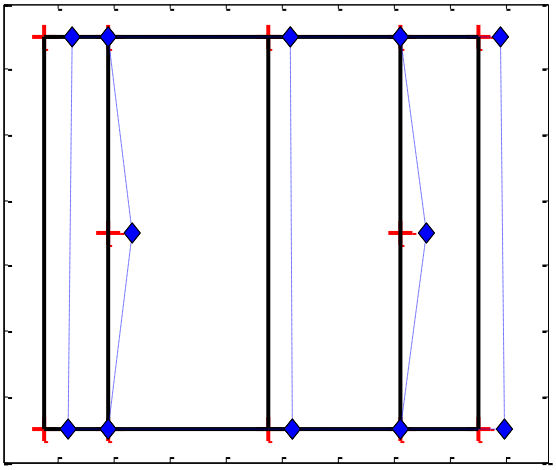

Figure 17: Fundamental longitudinal mode shape. T = 0.092 s.

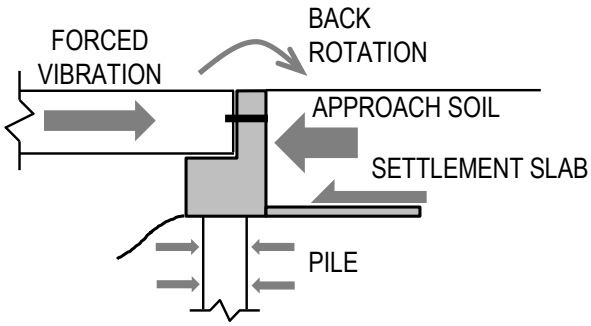

Figure 18: Schematic of force transfer mechanism in the longitudinal direction.

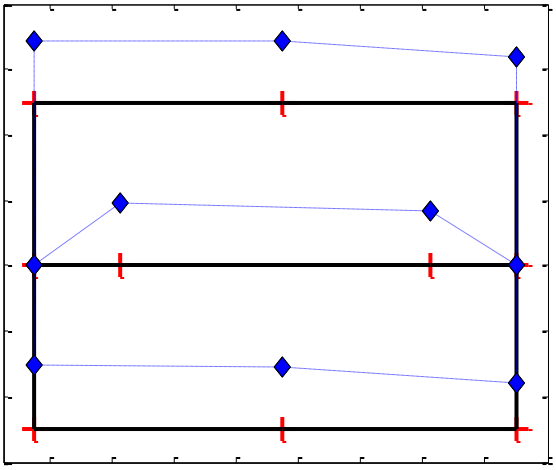

Figure 19: Fundamental transverse mode shape. T = 0.118 s.

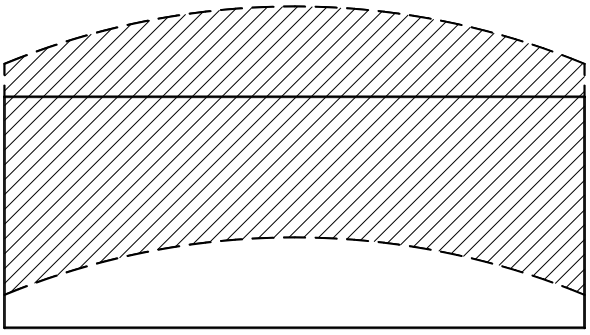

SYMMETRICAL ABUTMENTS

a) Translational deck movement allowed by settlement slabs.

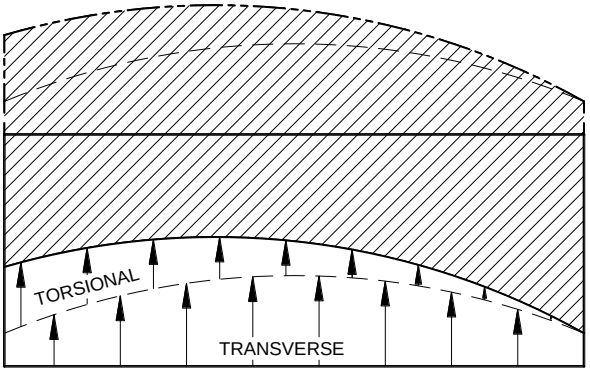

GAPPING AT WEST ABUTMENT

b) Torsional movement arising from different pile foundation stiffnesses.

Figure 20: Components of transverse mode shape.

In the transverse direction, the bridge had a natural period of 0.118 s. This mode shape was primarily translational with a smaller torsional component that resulted in a rotational movement centred around the southern end of the undamaged eastern abutment (Figure 19). Modal amplitudes at the western abutment were 30% higher than those at the eastern abutment and were only slightly less than the modal amplitudes at mid span. The increased flexibility at the western abutment was from lateral spreading induced soil gapping at the pile faces as explained previously. This variance in modal amplitude between the two abutments clearly demonstrates that in the transverse direction, the soil mass behind the abutment had a smaller effect on the dynamic response when compared to the response in the longitudinal direction. Without wing-walls at the abutment to provide passive resistance in the transverse direction, the only resistance apart from the pile foundations comes from the frictional resistance along the backwall of the abutment at the soil-abutment interface and the friction between the settlement slab and the approach fill. In an earthquake, the contribution from the backwall frictional resistance would be reduced as gapping developed behind the abutment. The stiffness of the pile foundations provided the dominant contribution to the substructure stiffness, with the stiffness from relative movement between the soil and the settlement slab contributing to a lesser extent.

A schematic comparison of the mode shape from this testing, and the mode shape expected if no lateral spreading had occurred is shown in Figure 20. If no gaps had developed, then the foundation system response would have most likely been symmetrical about the transverse axis of the bridge, with translation of the bridge deck and some rotation in plan at each abutment (Figure 20a). Prior to the Darfield earthquake, both approach fills were at a similar elevation and the top few metres of surface soils that would have controlled the stiffness of the overall abutment system had similar characteristics.

However as only one approach had suffered damage, torsional modal behaviour would be expected. If only pile stiffness was considered, the eastern abutment would act effectively rigid when compared with the western abutment and the bridge would be expected to have a mode shape dominated by torsion, but the 2.0 m friction slab at either abutment provided enough stiffness to the substructure to make the dominant movement in the transverse direction translational rather than torsional. Because of the reduced stiffness of the western abutment pile foundations, the response is representative of that shown in Figure 20b, with the transverse and torsional components of the response highlighted.

CONCLUSIONS

Forced vibration testing of the Davis Road Bridge was able to capture modal properties in both principal lateral directions of the bridge after the western approach and abutment were damaged by liquefaction induced lateral spreading. Testing of this simple structure allowed the abutment response to be isolated, and the stiffness contribution of the different components of the substructure to be investigated. These modal properties were extracted using a rigorous two phase identification process. In the first phase, modal properties were extracted from force-normalized test data. As force input was not directly measured, a methodology to approximate input force from nearby acceleration channels was presented. The second phase of modal extraction used a portion of the non-force-normalized acceleration records that centred on the true modes identified in the first phase. The collection and analysis of this in-situ data was made possible by the use of SIT and the suite of system identification algorithms it utilizes. This process provided robust identification of mode shapes that resulted in a clear overview of the stiffness contributions of various substructure components on the dynamic response of the bridge. In the longitudinal direction, the approach soil dominated the response, as indicated by the symmetrical response of the structure in this direction. In the transverse direction, the effect of the gapping around the foundations in the western approach was indicated by the torsional component of the identified mode. These results showed that in the transverse direction the pile foundation system, rather than the approach soil, was the dominant contributor to the overall stiffness of the substructure.

This testing is part of a larger suite of forced vibration testing of full scale bridge structures. Testing of the response of isolated bridge components and complete in-service bridges has been undertaken to develop a better understanding of the in-situ response of bridges and the interaction between the various structural and foundation components. Results from the forced vibration testing of simple structures such as the Davis Road Bridge will be used to inform the testing and analysis of more complex systems where load sharing between abutments and piers will be evident.

ACKNOWLEDGMENTS

The authors would like to extend their thanks to Selwyn District Council, HEB Construction, the University of Canterbury, and Kimberley Twigden for providing access to the bridge, the donation of equipment and personnel time, and logistical support. We acknowledge the New Zealand GeoNet project and its sponsors EQC, GNS Science and LINZ, for providing ground motion records used in this study.

REFERENCES

1 El-Gamal, M. and R.V. Siddharthan, (1998). "Stiffnesses of Abutments on Piles in Seismic Bridge Analyses". *Soils and Foundations*, **38** (1): 77-87.

2 Kotsoglou, A. and S. Pantazopoulou, (2009). "Assessment and Modeling of Embankment Participation in the Seismic Response of Integral Abutment Bridges". *Bulletin of Earthquake Engineering*, **7** (2): 343-361.

3 Zhang, J. and N. Makris, (2002). "Seismic Response Analysis of Highway Overcrossing Including Soil-Structure Interaction". *Earthquake Engineering and Structural Dynamics*, **31** (11): 1967-1991.

4 Stewart, J.P., E. Taciroglu, J.W. Wallace, E.R. Albergh, A. Lemnitzer, C. Rha, and P.K. Tehrani, (2007). "Full Scale Cyclic Testing of Foundation Support Systems for Highway Bridges. Part II: Abutment Backwalls". (UCLA-SGEL Report 2007/02).

5 Aviram, A., K.R. Mackie, and B. Stojadinovic, (2008). "Effect of Abutment Modeling on the Seismic Response of Bridge Structures". *Earthquake Engineering and Engineering Vibration*, **7** (4): 395-402.

6 Goel, R.K. and A.K. Chopra, (1997). "Evaluation of Bridge Abutment Capacity and Stiffness During Earthquakes", *Earthquake Spectra*. **13** (1): 1-23.

7 Anastasopoulos, I., T. Georgarakos, V. Georgiannou, V. Drosos and R. Kourkoulis, (2010). "Seismic Performance of Bar-Mat Reinforced-Soil Retaining Wall: Shaking Table Testing Versus Numerical Analysis with Modified Kinematic Hardening Constitutive Model". *Soil Dynamics and Earthquake Engineering*, **30** (10): 1089-1105.

8 Johnson, N., R.T. Ranf, M.S. Saiidi, D. Sanders and M. Eberhard, (2008). "Seismic Testing of a Two-Span Reinforced Concrete Bridge". *Journal of Bridge Engineering*, **13** (2): 173-182.

9 Moss, P.J., A.J. Carr and G.C. Pardoen, (1982). "The Vibrational Behaviour of Three Composite Beam-Slab Bridges". *Engineering Structures*, **4** (4): 277-288.

10 Samman, M.M. and M. Biswas, (1994). "Vibration Testing for Nondestructive Evaluation of Bridges. I: Theory". *Journal of Structural Engineering*, **120** (1): 269-289.

11 Bolton, R., C. Sikorsky, S. Park, S. Choi and N. Stubbs, (2005). "Modal Property Changes of a Seismically Damaged Concrete Bridge", *Journal of Bridge Engineering*. **10** (4): 415-428.

12 Halling, M.W., I. Muhammad, and K.C. Womack, (2001). "Dynamic Field Testing for Condition Assessment of Bridge Bents". *Journal of Structural Engineering*, **127** (2): 161-167.

13 Elgamal, A.W., S. Alampalli and P. Van Laak, (1996). "Forced Vibration of Full-Scale Wall-Backfill System". *Journal of Geotechnical and Geoenvironmental Engineering*, **122** (10): 849-858.

14 Wilson, P. and A. Elgamal, (2009). "Full-Scale Shake Table Investigation of Bridge Abutment Lateral Earth Pressure". *Bulletin of the New Zealand Society for Earthquake Engineering*, **42** (1): 39-46.

15 Crouse, C.B., B. Hushmand and G.R. Martin, (1987). "Dynamic Soil-Structure Interaction of a Single-Span Bridge". *Earthquake Engineering & Structural Dynamics*, **15** (6): 711-729.

16 Site Investigation Ltd., (2004). "Piezocone Penetrometer Test (CPTU) Report: Davis Road".

17 Palermo, A., M.L. Heux, M. Bruneau, M. Anagnostopoulou, L. Wotherspoon and L. Hogan, (2010). "Preliminary Findings on Performance of Bridges in the 2010 Darfield Earthquake". *Bulletin of the New Zealand Society for Earthquake Engineering*, **43** (4): 412-420.

18 Yashinsky, M. and M.J. Karshenas, (2003). *Fundamentals of Seismic Protection for Bridges*. Earthquake Engineering Research Institute, Oakland, CA.

19 Youd, T.L., I.M. Idriss, R.D. Andrus, I. Arango, G. Castro, J.T. Christian, R. Dobry, W.D. Liam Finn, Harder L.F, Jr., M.E. Hynes, K. Ishihara, J.P. Koester, S.S.C. Liao, W.F. Marcuson III, G.R. Martin, J.K. Mitchell, Y. Moriwaki, M.S. Power, P.K. Robertson, R.B. Seed and K.H. Stokoe II, (2001). "Liquefaction Resistance of Soils: Summary Report from the 1996 NCEER and 1998 NCEER/NSF Workshops on Evaluation of Liquefaction Resistance of Soils". *Journal of Geotechnical and Geoenvironmental Engineering*, **127** (10): 817-833.

20 GNS Science, (2012). *Geonet*. Accessed: September 20, 2012, http://www.geonet.org.nz.

21 Wotherspoon, L., A. Bradshaw, R. Green, C. Wood, A. Palermo, M. Cubrinovski and B. Bradley, (2011). "Performance of Bridges During the 2010 Darfield and 2011 Christchurch Earthquakes". *Seismological Research Letters*, **82** (6): 950-964.

22 Beskhyroun, S., (2011). "Graphical Interface Toolbox for Modal Analysis". in *Ninth Pacific Conference on Earthquake Engineering*: Auckland, New Zealand.

23 Brincker, R., L. Zhang and P. Andersen, (2001). "Modal Identification of Output-Only Systems Using Frequency Domain Decomposition". *Smart Materials and Structures*, **10** (3): 441-445.

24 Jacobsen, N.J., P. Andersen, and R. Brincker, (2007). "Using EFDD as a Robust Technique to Deterministic Excitation in Operational Modal Analysis". In *The 2nd International Operational Modal Analysis Conference (IOMAC)*: Copenhagen, Denmark.

25 Katayama, T., (2005). *Subspace Methods for System Identification*. Springer, London.

26 Allemang, R.J., (2003)."The Modal Assurance Criterion - Twenty Years of Use and Abuse". *Sound and Vibration*, **37** (8): 14-21.